



OPEN ACCESS

EDITED BY

Lucia Baldino,
University of Salerno, Italy

REVIEWED BY

Abdelghani Saouab,
University of Le Havre, France
Veronique Michaud,
Ecole polytechnique Fédérale de
Lausanne, Switzerland

*CORRESPONDENCE

Florence Saffar,
florence.saffar@onera.fr

SPECIALTY SECTION

This article was submitted to Polymeric
and Composite Materials,
a section of the journal
Frontiers in Materials

RECEIVED 02 September 2022

ACCEPTED 27 October 2022

PUBLISHED 23 November 2022

CITATION

Saffar F, Beauchêne P, Sonnenfeld C and
Park CH (2022), Influence of prepreg
parameters on the interlaminar
consolidation of fiber reinforced
thermoplastic laminates manufactured
by vacuum-bag-only process.
Front. Mater. 9:1035427.
doi: 10.3389/fmats.2022.1035427

COPYRIGHT

© 2022 Saffar, Beauchêne, Sonnenfeld
and Park. This is an open-access article
distributed under the terms of the
[Creative Commons Attribution License
\(CC BY\)](#). The use, distribution or
reproduction in other forums is
permitted, provided the original
author(s) and the copyright owner(s) are
credited and that the original
publication in this journal is cited, in
accordance with accepted academic
practice. No use, distribution or
reproduction is permitted which does
not comply with these terms.

Influence of prepreg parameters on the interlaminar consolidation of fiber reinforced thermoplastic laminates manufactured by vacuum-bag-only process

Florence Saffar^{1,2*}, Pierre Beauchêne¹, Camille Sonnenfeld¹
and Chung Hae Park²

¹DMAS, ONERA, Université Paris-Saclay, F-92322, Châtillon, France, ²Center for Materials and Processes, IMT Nord Europe, Institut Mines-Télécom, Université de Lille, Lille, France

To better understand the influence of the prepreg parameters such as surface roughness, fibres/matrix distribution (e.g. presence or absence of pure matrix layer on the prepreg surface) and initial matrix crystallinity, two different carbon fibres/Poly-Ether-Ketone-Ketone prepreps are used to fabricate unidirectional laminate by Vacuum-Bag-Only (VBO) process. By an *in-situ* monitoring set-up, the laminate thickness and the temperature difference along the thickness direction are measured throughout the consolidation cycle. The quality of laminate is assessed in terms of interlaminar shear strength and void content. A finite element model has been developed to describe the intimate contact establishment by the deformation of surface roughness between the glass transition temperature and the melting temperature of the matrix. In particular, the model takes into account the real profilometer data and the variable Young's modulus of matrix in terms of temperature and crystallinity. Finally, the high influence of the matrix crystallinity degree and the surface roughness on the intimate contact phenomenon is highlighted.

KEYWORDS

intimate contact, thermoplastic composite, VBO, crystallinity, prepreg roughness, interlaminar consolidation

1 Introduction

In the aeronautic sector, the use of thermoplastic composites for aircraft design is constantly growing. In addition to their good mechanical properties such as toughness and impact resistance, their short manufacturing cycle and the possibility of melt welding give them a lead on their thermoset counterparts such as carbon/epoxy composites (Stewart, 2011; Costa et al., 2012; Marsh, 2014; McIlhagger et al., 2015; Soutis et al., 2020). All these properties represent major advantages to face up the rising production volume in the aircraft sector. Moreover, high performance thermoplastic polymers are required for the composites adopted by the aeronautic industry, such as Poly-Ether-Ether-Ketone

(PEEK) or Poly-Phenyl-Sulphide (PPS) which offer higher environmental resistance (Schuhler et al., 2018), (Dubary et al., 2017). In this context, Poly-Ether-Ketone-Ketone (PEKK) is attracting great interest as a promising alternative to PEEK, because it offers a better temperature resistance owing to a higher glass transition temperature, while it has a similar manufacturing condition because of the same range of melting temperature as that of PEEK (Hsiao et al., 1991; Gardner et al., 1992; Krishnaswamy and Kalika, 1996; Wypych and Wypych, 2016; Choupin, 2017; Tadini et al., 2017; Choupin et al., 2018; Li and Strachan, 2019; Judovits, 2020).

In parallel with these material developments, the manufacturing methods should also be improved to respond to the economic and technical challenges of the aeronautic sector. For the present, the autoclave process is still the principal manufacturing route to produce aeronautic composite structures with high fibre volume fraction and low void content (Lystrup and Andersen, 1998), (Patou et al., 2019). However, this manufacturing method is expensive and extremely energy consuming, especially due to the high pressure required for the consolidation process. Besides, the maximum product size is limited by the autoclave size which determines the equipment purchase and maintenance costs. For all these reasons, new consolidation ways such as thermoforming (Sadighi et al., 2008; Chen et al., 2011; Wang et al., 2013; Akkerman et al., 2015; Guzman-Maldonado et al., 2016; Margossian et al., 2016), overmoulding (Akkerman et al., 2020), (Liebsch et al., 2019) automated tape placement with *in-situ* consolidation (Qureshi et al., 2014; Stokes-Griffin and Compston, 2015; Bandaru et al., 2019; Engelhardt et al., 2019), tape winding (Tannous et al., 2016), vacuum-bag-only (VBO) or out-of-autoclave (OoA) process (Ijaz et al., 2007), (Saffar et al., 2020) have been developed and investigated.

In particular, vacuum-bag-only process offers many advantages in terms of usage, design and adaptability. In this manufacturing route, composite laminates are consolidated at very low pressures (<1 bar). Even if a good consolidation quality can be obtained by this process (Saffar et al., 2020), the influence of a reduced pressure on the interlaminar consolidation phenomena (intimate contact (Loos and Dara, 1987; WooLee and Springer, 1987; Cassidy and Monaghan, 1994; Butler et al., 1998; Yang and Pitchumani, 2001; Khan et al., 2010; Levy et al., 2013; Schaefer et al., 2017; Çelik et al., 2020), autohesion or healing (WooLee and Springer, 1987), (De Gennes and Georges, 1981; Mantell and Springer, 1992; Lamèthe et al., 2005; Régnier et al., 2005; Mulye et al., 2020), melt flow (Barnes and Cogswell, 1989; Groves and Stocks, 1991; Stanley and Mallon, 2006; Picher-Martel et al., 2017), crystallisation (Ijaz et al., 2007), (Guan and Pitchumani, 2004a; Guan and Pitchumani, 2004b; Tierney and Gillespie, 2004; Dörr et al., 2019; Martineau et al., 2019)) is still not fully understood.

In this context, industrial prepreg materials for OoA processes have been developed in order to ensure good

TABLE 1 Characteristic temperatures of PEKK matrix.

Tg (°C)	155
Tm (°C)	335
Tcc (°C)	180–230
Tc (°C)	250–310

Tg: Glass transition temperature.

Tm: Melting temperature.

Tcc: Cold crystallisation temperature.

Tc: Crystallisation temperature.

mechanical properties of a final laminate in spite of the weak consolidation pressure. Some particular features for such thermoset prepreps are the presence of voids evacuation paths (Kratz and Hubert, 2013; Kourkoutsaki et al., 2015; Levy et al., 2015), a sudden decrease of the matrix viscosity above a precise temperature (Kim et al., 2014), a high transverse permeability in the through thickness direction (Grunenfelder et al., 2017; Schechter et al., 2018; Schechter et al., 2020) and the use of partially polymerised matrix (Shin et al., 2019). Contrary to the development of these thermoset prepreg materials, the criteria for OoA thermoplastic prepreg that ensure a good interlaminar consolidation under low pressure have not been totally identified.

The objective of this work is to investigate the influence of prepreg parameters such as prepreg surface roughness and matrix crystallinity on the interlaminar consolidation phenomena during low pressure consolidation processes such as VBO or OoA processes. In this work, two different carbon fibres/PEKK prepreg materials that are designed for autoclave consolidation processes are compared. So far, the intimate contact establishment has been predicted by analytical models assuming the surface roughness as a rectangular shape, in the literature (Loos and Dara, 1987; WooLee and Springer, 1987; Butler et al., 1998). The shape of the real prepreg surface roughness is, however, far from being rectangular. This oversimplification may be one of the reasons for the discrepancy between the model prediction and the experimental data. In this work, the real profile of surface roughness is used in the finite element modelling of intimate contact using the material properties depending on the temperature and the crystallinity degree.

2 Materials and methods

2.1 Two kinds of prepreps

2.1.1 General presentation

Two unidirectional continuous carbon fibres/Poly-Ether-Ketone-Ketone (PEKK) prepreg materials (denoted as Prepreg A and Prepreg B without denoting the grade and the supplier for confidentiality reasons) from two

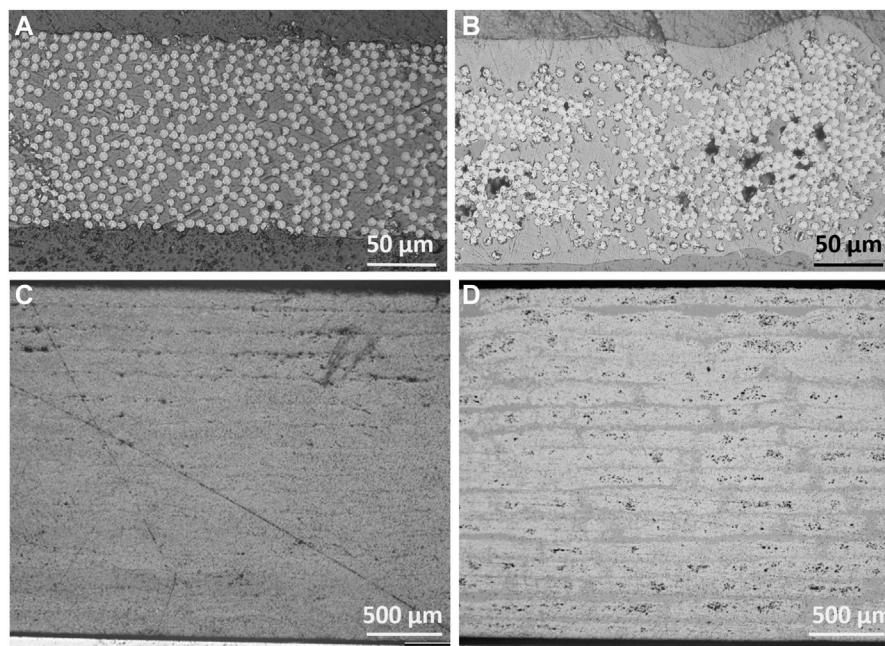


FIGURE 1
Microscopic observations of prepregs ((A) Prepreg A (B) Prepreg B) and 16 plies UD laminate ((C) Prepreg A (D) Prepreg B) cross sections.

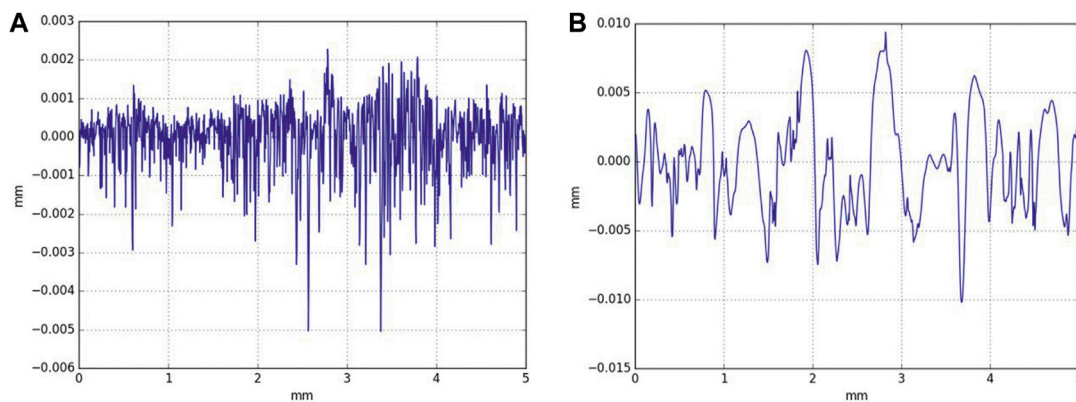


FIGURE 2
Profilometric study of both prepregs (A) Prepreg A (B) Prepreg B.

different suppliers were used. These prepreg materials are different in terms of surface roughness and initial crystallinity of matrix, which are described in the subsequent sections. The thermal properties of PEKK are summarised in Table 1. Both of these prepregs have the same matrix mass fraction (34%) and the same fibre areal weight (145 gm). A microscopic observation of the cross section of these prepreg sheets are presented in Figure 1 which underlines different fibres distribution, surface roughness

and void content. No porosity was observed microscopically in Prepreg A. On the other hand, the void content (i.e. void area fraction on the prepreg cross section) of Prepreg B that was evaluated by a thresholding method on ImageJ (<https://imagej.nih.gov/ij/>), was around 7% ($\pm 3.2\%$). Moreover, in the case of Prepreg B, a pure matrix layer without fibres is found at each surface of the prepreg, while carbon fibres are uniformly distributed along the cross section (even on the surface) of Prepreg A.

TABLE 2 Crystallinity degrees of three different prepreg samples.

Samples	Crystallinity degree (evaluated by DSC)
a (%): Quasi-amorphous prepreg	3
b: Initial prepreg	13
c: High-crystalline prepreg	31

2.1.2 Surface roughness

The surface roughness of the prepreg was analysed by a contact profilometer (*Mahr MarSurf M400*). The measurement speed was 0.50 mm/s and the measurement distance step was 0.4 μm . The measurement was made in the transverse direction to the fibres. The roughness of both surfaces of each prepreg was measured and no difference between the top and bottom surfaces was observed. The prepreg roughness profiles are presented in Figure 2. A periodic shape of roughness profile can be observed for Prepreg A whereas such periodic shape is not shown for Prepreg B. Moreover, there is a big difference in terms of roughness height between the two prepreg materials. The mean height of the surface roughness for Prepreg A is around 3.5 μm which corresponds to the radius of carbon fibre. The mean surface roughness for Prepreg B is more than twice greater i.e. about 7.5 μm . In particular, a pure matrix layer without carbon fibres is present on the top and bottom surfaces of Prepreg B, whereas carbon fibres are uniformly distributed on the cross section of Prepreg A (see Figure 2).

2.1.3 Initial crystallinity of matrix

As the initial crystallinity degree of both prepreg materials was similar around 13%, heat treatment was applied on the prepreps to obtain different prepreg samples with three crystallinity degrees: quasi-amorphous material (a), intermediate crystallinity degree material (i.e. initial as-received prepreg without heat treatment) (b) and high-crystalline material (c). The quasi-amorphous prepreg samples were obtained by melting the initial Prepreg B at 360°C (around $T_m+25^\circ\text{C}$) during 15 min to erase the thermal history and to melt crystallized forms. Then, they were quenched. The high-crystalline prepreg samples were obtained by heating the initial Prepreg B at 5K/min until 215°C that is in the range of the cold crystallization temperature and keeping it at this temperature for 60 min. The crystallinity degree of all these samples was evaluated by differential scanning calorimetry analysis. Table 2 summarizes the crystallinity degrees of these three samples.

The matrix crystallinity degree has a high influence on the mechanical properties of the material (Xu et al., 2001; Blond et al., 2014; Batista et al., 2016; Talbott et al., 2016; Armagan, 2020), and in particular its influence on the Young's modulus was studied by Choupin (Choupin, 2017) in the case of PEKK matrix.

The Young's modulus of PEKK rises with increasing crystallinity degree at room temperature as well as at 180°C (around $T_g + 25^\circ\text{C}$) as shown in Figure 3.

2.2 Manufacturing and monitoring methods

2.2.1 VBO consolidation with a one sided heating plate

The laminates consolidation was performed by VBO manufacturing. The chosen lay-up was a hand lay-up of 16 unidirectional layers. The prepreg stack was set under vacuum bag which allowed to apply -995 mbar pressure throughout the consolidation cycle. The heating set-up was a heating plate monitored by Eurotherm apparatus and the laminate was only heated by the bottom side. Currently, this kind of one sided heating tool is employed in the aeronautic industry to manufacture large structures to avoid the part size limitation in the case of autoclave or heat oven heating processes. For an industrial manufacturing of thick structures, however, such a system may be adapted by adding a superior heat source (as IR heat). Moreover, in this work, this set-up allowed to ease the process monitoring described below. The applied temperature cycle was a 5 K/min heating rate up to a temperature plateau at 360 °C. This plateau was maintained for 15 min and followed by a free cooling.

2.2.2 Monitoring set-up

In order to monitor the consolidation phenomena, an experimental set-up as described by Saffar et al. (Saffar et al., 2020) was used (see Figure 4). K-type thermocouples were placed on the top and bottom sides of the laminates to measure temperature difference through the laminate thickness during the consolidation cycle. Digital image correlation (DIC) was performed on the top surface of the laminate to monitor the variation of the laminate thickness.

2.3 Assessment of laminate quality by interlaminar shear strength (ILSS)

The interlaminar consolidation quality was assessed by interlaminar shear strength which was evaluated by short beam shear test. The mechanical tests were conducted on Zwick/Roell Z010 with a load cell of 10 kN. The rectangular sample dimensions were around 25 mm \times 12 mm with a thickness of 2.35 mm. The radius of the two supporting pins was 2 mm and the radius of the loading pin was 5 mm. The distance between the two supporting pins was 12 mm. The displacement speed of the loading pin was 0.5 mm/min.

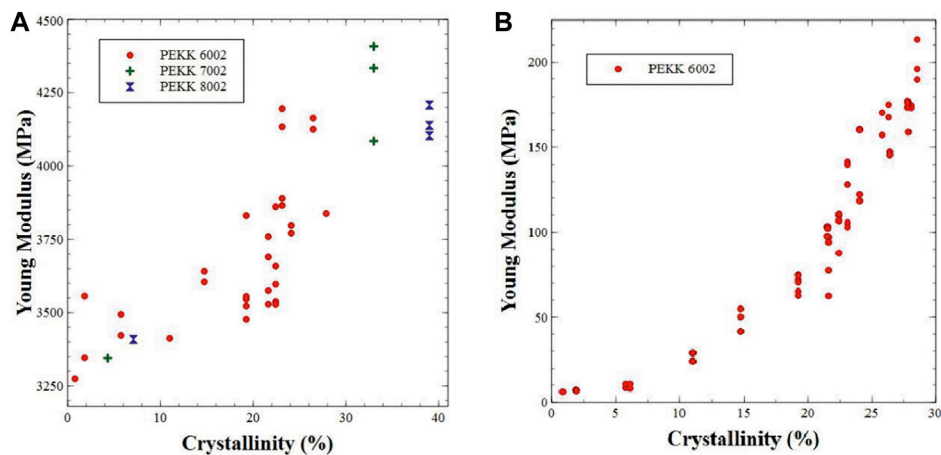


FIGURE 3 Young's modulus against crystallinity degree for PEKK (Choupin, 2017) (A) $T = T_{amb}$ (B) $T = 180\text{ }^{\circ}\text{C} (>T_g)$.

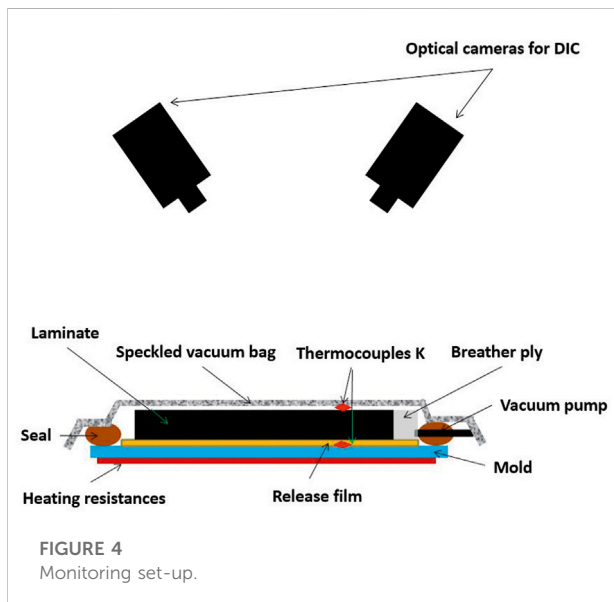


FIGURE 4 Monitoring set-up.

2.4 Finite element modelling of intimate contact

2.4.1 General presentation

The influence of surface roughness and matrix crystallinity degree on the interlaminar consolidation phenomena was modelled by two dimensional finite element simulations using the commercial software Comsol Multiphysics. The intimate contact establishment between two adjacent prepreg sheets below the melting temperature was simulated as a contact between an extremely rigid flat plate and a deformable material with a

rough surface. Under the compacting pressure, the deformation of rough surface was calculated and the increase of contact surface was obtained. The challenge of this numerical simulation was the multiple contact points which led to a difficulty in the numerical convergence.

In order to simplify the model, only the mechanical properties of the material were considered as a function of temperature, whereas the heat conduction simulation was not performed and the experimental temperature data was implemented as the input data in the numerical simulation.

2.4.2 Geometry and material properties

The numerical geometry of the model for both prepreg materials are presented in Figure 5. The surface roughness profiles of the prepreg in the numerical model corresponded to the experimental data obtained by profilometric study (see the aforementioned Section 2.1.2). Young's modulus values of PEKK were taken from the Choupin's study for the three crystallinity degrees: 3%, 13% and 31%. A step evolution of the Young's modulus between room temperature value and 160°C value in a function of time (hence in a function of temperature, as the temperature was changed with time according to the consolidation cycle) was selected (see Table 3 and Figure 3). This modulus evolution follows a sigmoid function with a 800 s-transition zone.

2.4.3 Boundary conditions

Different boundary conditions were applied on the model system (i.e. rigid plate and prepreg sheet). A roller condition was applied on the bottom side of the prepreg and a symmetry condition was imposed on the left side of the

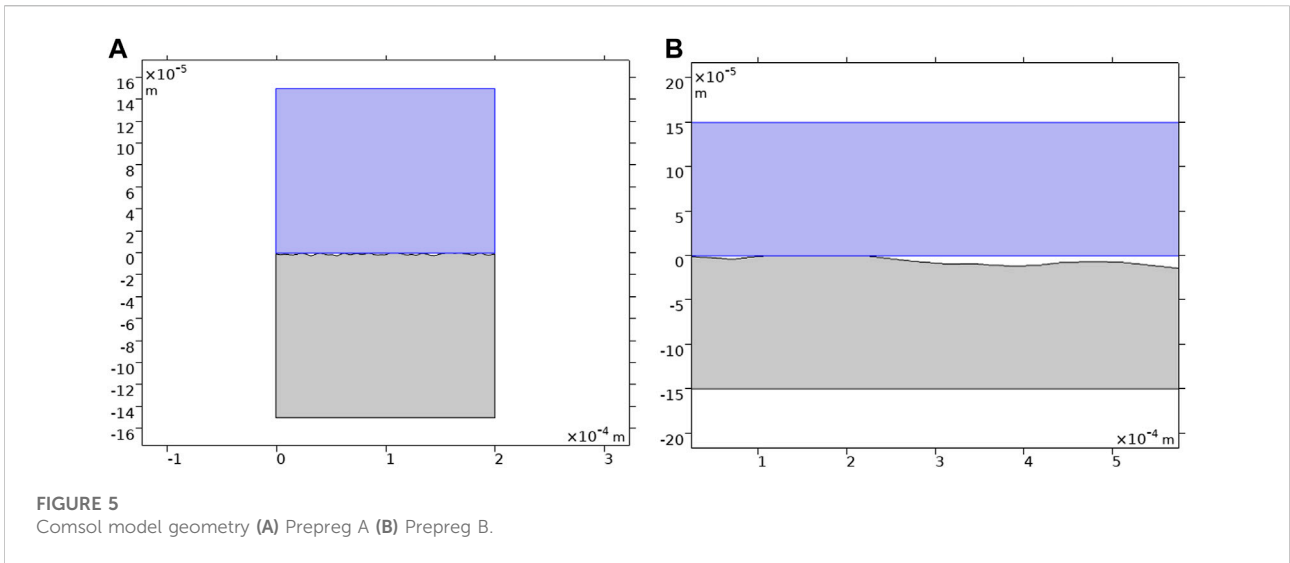
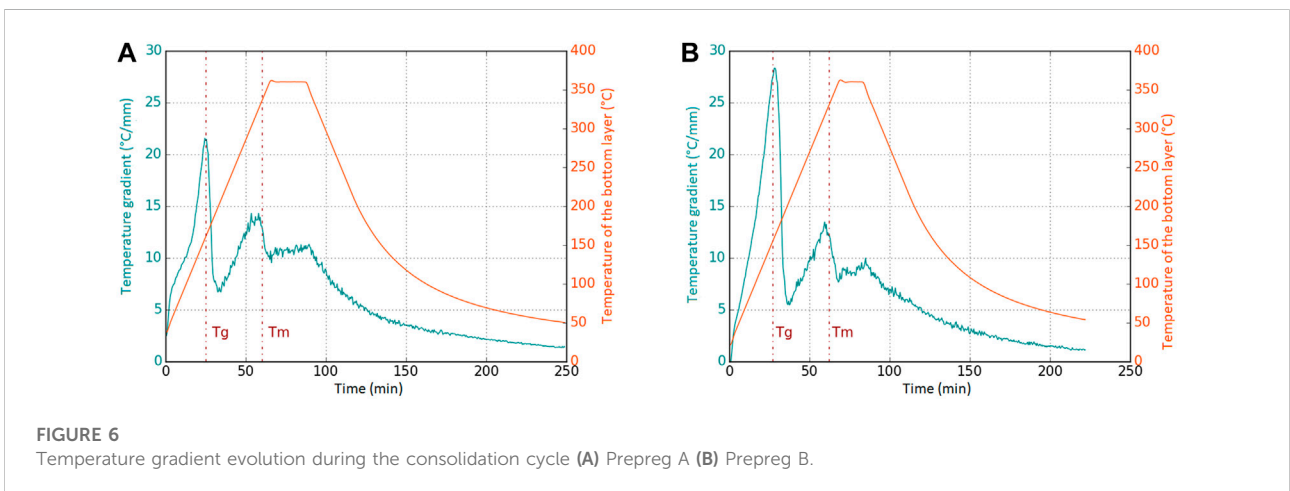


TABLE 3 Young’s modulus for different temperatures and crystallinity degrees.

	Young’s modulus value under T _g (GPa)	Young’s modulus value above T _g (MPa)
A: Quasi-amorphous material	3.35	8.00
B: Initial material	3.40	25.00
C: High-crystalline material	4.00	23.80



whole system. Symmetric conditions were also applied to consider a prepreg half-thickness. Contact pair was created between the rough surface of the prepreg and the bottom side of the rigid plate.

To reproduce the vacuum pressure condition, 1 bar pressure was applied on the top side of the rigid plate. To achieve a model convergence this load was applied according to a step evolution from zero to 1 bar in 0.1 s.

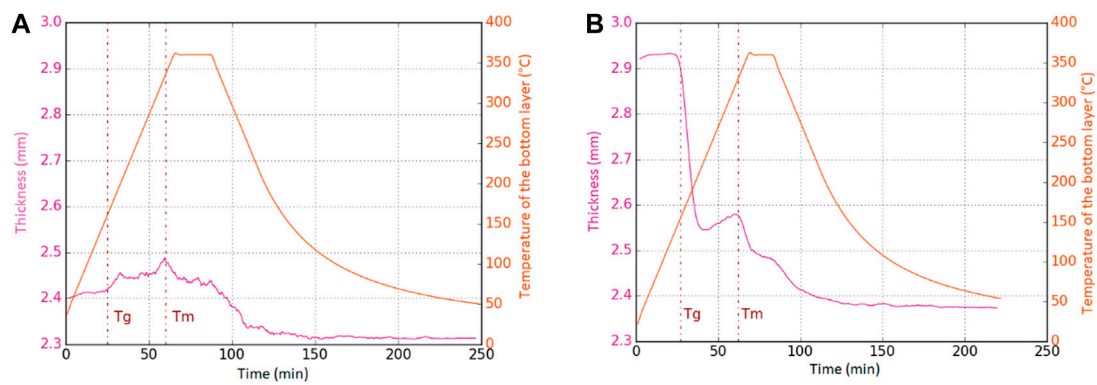


FIGURE 7
Thickness evolution during the consolidation cycle (A) Prepreg A (B) Prepreg B.

3 Experimental results

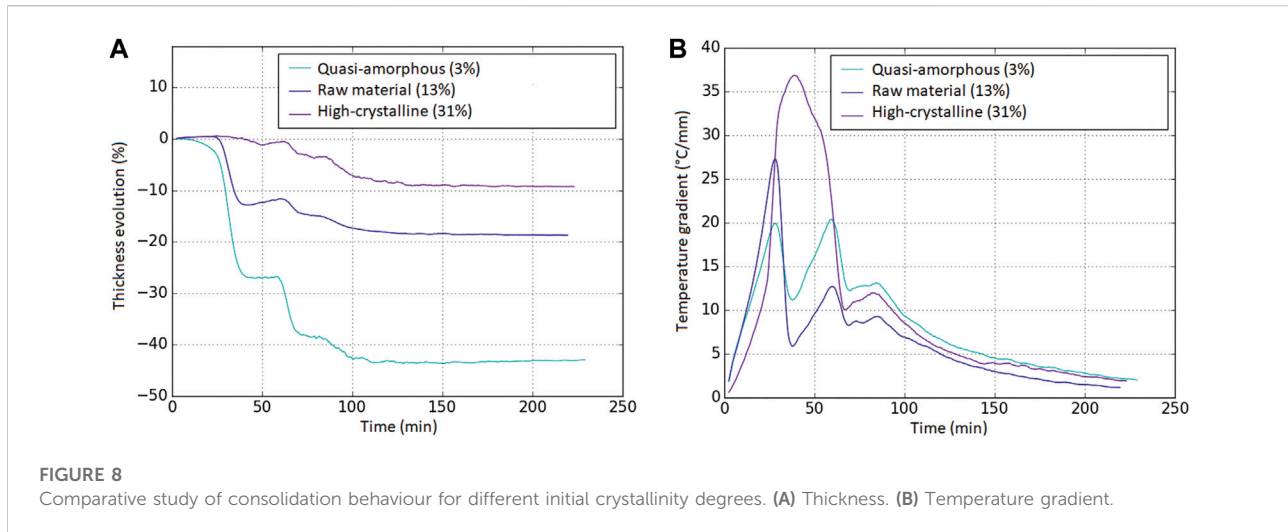
3.1 Influence of surface roughness

It should be noted that the average temperature gradient was obtained by dividing the temperature difference between the top and bottom surfaces by the laminate thickness. Figure 6 shows a similar thermal behaviour for both prepreg materials: a significant decrease of the average temperature gradient at T_g and a small drop at T_m . These two phenomena are respectively associated to intimate contact phenomenon and to the flow of molten composite (Saffar et al., 2020). The higher value of the temperature gradient at T_g for Prepreg B can be explained by its greater surface roughness and the corresponding greater empty area between the neighbouring prepreg layers. The thermal contact resistance at the interfaces between two adjacent layers is more important for Prepreg B. Figure 7 presents the laminate thickness evolution during the consolidation cycle for both prepreg materials. At T_g a very different behaviour can be observed for the two prepreg materials. In the case of Prepreg A, the laminate thickness still increased above the T_g , while in the case of Prepreg B the laminate thickness highly decreased by around 12.5%. Until T_m the laminate thickness evolution of Prepreg A was in agreement with the transverse thermal expansion of the prepreg as described by Saffar et al. (Saffar et al., 2020).

According to the profilometric study of Prepreg B, the mean roughness height was $7.5 \mu\text{m}$ and the maximum roughness height was $25 \mu\text{m}$ which respectively represent around 8% and 28% of the prepreg half-thickness, respectively. On the other hand, the mean and the maximum roughness height values of Prepreg A represent around 4.5% and 7%, respectively. This great difference of surface roughness between the two prepreg materials and the presence of pure matrix layer on the surface of Prepreg B can explain this opposite behaviour of the two

prepreg materials at T_g . These hypotheses will be discussed in the subsequent sections of modelling results and discussion.

The interlaminar shear strength of both prepreg laminates was compared. For the same manufacturing condition, the interlaminar shear strength of the laminate from Prepreg B was around 17% lower than that from Prepreg A. The microscopic images of the cross section of the consolidated laminate (Figure 1-c-d) exhibit very different microstructures between materials A and B. In the first case (i.e. Prepreg A), no interface is visible between the adjacent layers on the lower part (i.e. close to the heating plate) of the laminate. In the 12th layers from the top, the void volume fraction was inferior to 2% and it reached 5% in the four top layers. Most of the voids were located at the interface between adjacent layers. The laminate from Prepreg B had a very different microstructure. Pure matrix layers without carbon fibres separated the neighbouring prepreg layers. Because carbon fibres were unevenly distributed in Prepreg B, the clusters (i.e. like tows) of fibres could be identified. Most of voids were found among the fibres, whereas the void volume fraction was almost the same value of around 4% through the thickness direction in the laminate. This void volume fraction in the final consolidated laminate is lower than that of the initial prepreg before manufacturing. This implies that internal voids can be removed during the OoA consolidation. Assuming that the difference of ILSS values between the two materials depends only on the voids, the ILSS value decreases by around 4% for each increase of 1% of void volume fraction. This order of magnitude is in agreement with the literature results about the influence of void on the ILSS for thermoset laminates (Olivier et al., 1995; Wisnom et al., 1996; Liu et al., 2006; Liu and Chen, 2016). Nevertheless, the influence of pure matrix layers at the prepreg surfaces on the interlaminar consolidation quality should be investigated further in a future work.

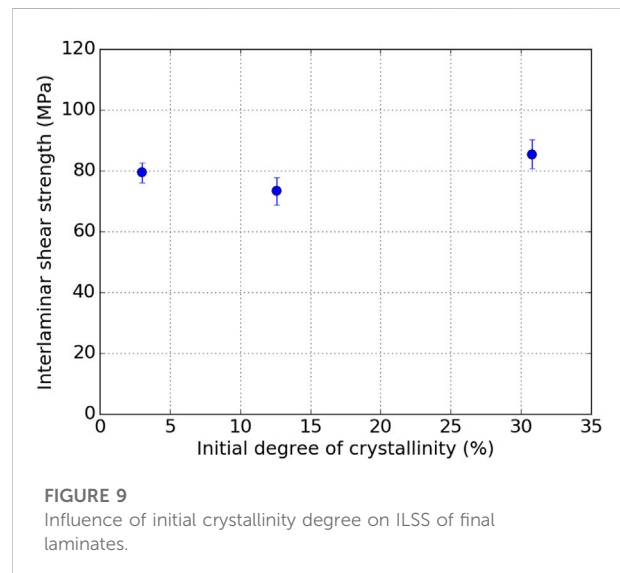


3.2 Influence of initial crystallinity degree

The monitoring set-up followed the evolutions of the laminate thickness and of the temperature gradient through the thickness during the consolidation cycle of 16 UD layer of quasi-amorphous, initial and high-crystalline Prepreg B samples. Figure 8A presents the laminate thickness evolution for these three crystallinity degrees. The more amorphous the matrix, the greater the variation of the laminate thickness. The decrease of laminate thickness at T_g was greater than 20% in the case of the quasi-amorphous material. Moreover, for the medium-crystalline (i.e. initial prepreg material without heat treatment) and the quasi-amorphous prepreg, the laminate thickness variation was much higher at T_g than at T_m . The influence of matrix melt flow was smaller than the surface roughness flattening during the intimate contact establishment.

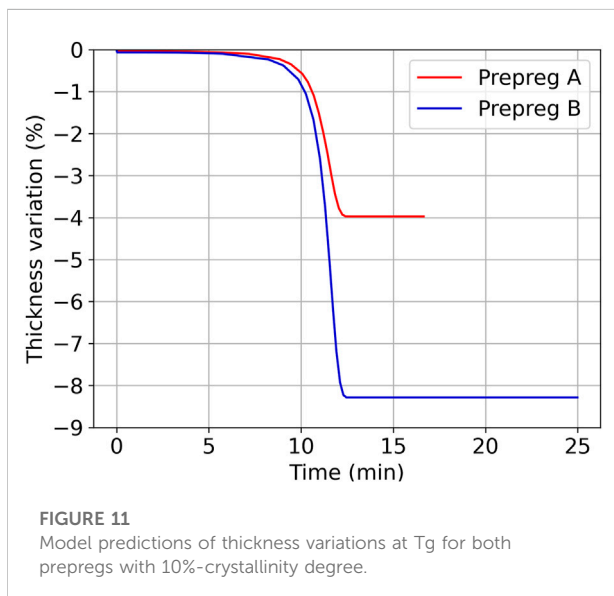
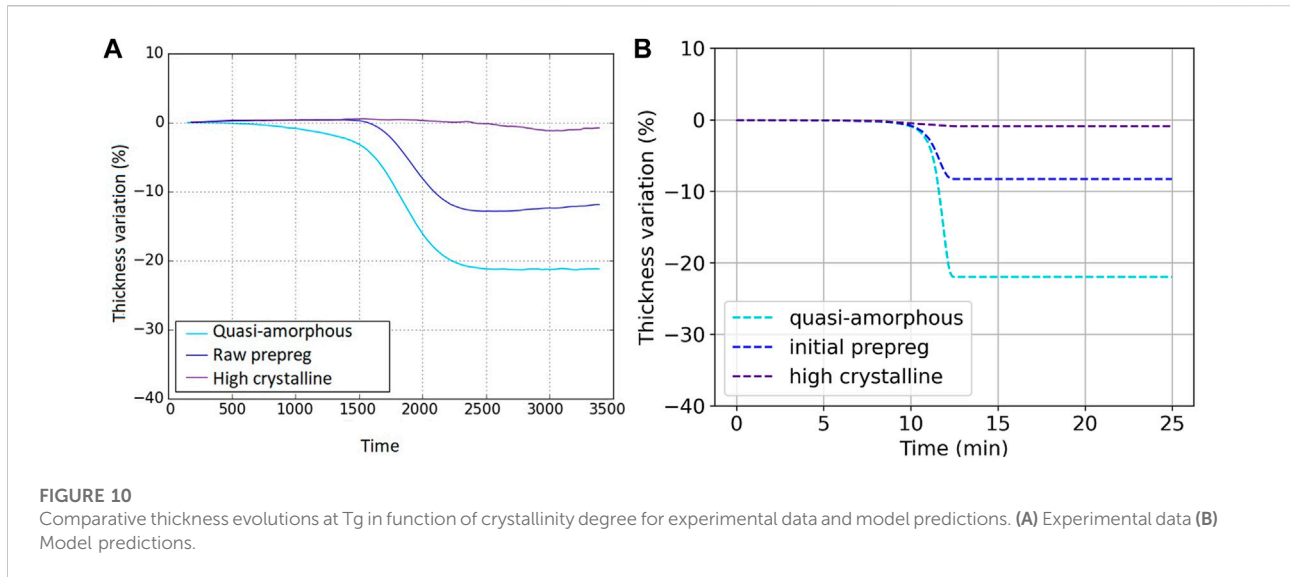
Figure 8B presents the average temperature gradient evolution for these materials. In the case of the high-crystalline material, no temperature gradient decrease was observed at T_g whereas significant change of the temperature gradient was observed for medium-crystalline and quasi-amorphous materials. At T_m , however, all three materials exhibited a similar behaviour. The temperature gradient decreased because the molten matrix filled the remaining gaps at the interlaminar interface, which increased the contact surface and decreased the thermal resistance. The higher value of the temperature gradient at T_g of quasi-amorphous prepreg than that of the medium-crystalline prepreg can be explained by the slight surface roughness distortion during the quench step. The interlocking of quasi-amorphous prepreg layers during the hand lay-up was more restricted than that of initial prepreg stack.

The absence of the temperature gradient drop in the case of the high-crystalline prepreg implies that there was no



improvement of the thermal conductivity at the interfaces between the adjacent layers. Thus, for high-crystalline materials, intimate contact was not established at T_g . Therefore, we can conclude that the surface roughness was not flattened due to the high elastic modulus of crystalline material or only amorphous molecules took part in autohesion or healing process while migrating across the interfaces.

The ILSS test results (see Figure 9) for these three laminates revealed a similar interlaminar consolidation quality. This result implies that the intimate contact can be completed by the molten matrix flow above the melting temperature even if the intimate contact is partial between the glass transition temperature and the melting temperature. This result could be predicted by



temperature gradient evolution which was the same for the three prepreg materials above the melting temperature.

4 Modelling results and discussion

By taking into account the real profile of the surface roughness of each prepreg, the 2D finite element model computed the surface roughness deformation and the corresponding change of the laminate thickness under a compaction pressure of 1 bar. It should be emphasized that the intimate contact establishment has been modelled by the viscous material flow of surface roughness above the melting

temperature in the literature. Nevertheless, it has been observed in our previous work (Saffar et al., 2020) that the intimate contact is built up between the glass transition temperature and the melting temperature where the viscosity is too great to induce the material flow. Hence, in this numerical simulation, the material was regarded as a solid material whose stiffness was represented by its Young's modulus which depends on the temperature and the crystallinity, and the deformation of surface roughness was computed by finite element simulation. Hence, this numerical model considered only the material deformation at T_g .

Figure 10 presents the comparison between the model predictions and the experimental data of laminate thickness variations at T_g of Prepreg B for three different crystallinity degrees. The more amorphous the material, the more important the thickness variation. These results underline that the greater intimate contact at T_g can be explained by the low Young's modulus at the rubbery state for quasi-amorphous material.

For a crystallinity degree of 10%, the laminate thickness for the two prepreg materials was predicted by the numerical simulation. The result presented in Figure 11 show that the deformation of Prepreg B was twice greater than that of Prepreg A (see Figure 11). This result is in agreement with the experimental data where a great thickness decrease happened at T_g for Prepreg B while the laminate thickness increased for Prepreg A. The model was able to predict that the surface roughness deformation had a bigger impact on the laminate thickness decrease for Prepreg B than for Prepreg A. Nevertheless, the limits of the numerical model could also be found by these results. Indeed, the model slightly underestimated the thickness decrease for prepreg B by predicting a decrease of 8.2% while the experimental value was around 12.5%. This difference could be caused by the presence of the matrix layer at the surface of the prepreg. The material property was not taken

on board by the model which could consequently consider a bi-phase material to describe Prepreg B. Moreover, the thermal expansion of the laminate should be taken into account by heat transfer simulation. This model improvement would allow to improve the thickness prediction. The numerical challenge is to deal with many points of contact however, and to define the mechanical and thermal properties of the interface between the prepreg layers in a future work.

5 Conclusion and perspectives

This work focused on the influence of the prepreg parameters such as surface roughness, fibre/matrix distribution (i.e. existence or absence of pure matrix layer on the prepreg surface) and initial crystallinity of matrix. The *in-situ* monitoring of temperature difference and laminate thickness was performed to obtain the experimental data of time-dependent temperature gradient and laminate thickness.

It has been found that the surface roughness influences the intimate contact phenomenon at T_g. In the case of very rough prepreg surface, the intimate contact phenomenon of adjacent layers can be detected by the laminate thickness variation while for smooth surface prepreg the monitoring of the laminate thickness will be insufficient to control the manufacturing process. Only the temperature monitoring (temperature difference or temperature gradient through the thickness) permits the comprehensive understanding of the interlaminar consolidation phenomena.

The influence of the initial crystallinity degree of matrix was also examined. No temperature gradient decrease can be observed at T_g for high-crystalline prepreg. Moreover, the reduction of the laminate thickness at T_g becomes greater with increasing amorphous parts in the matrix. These experimental data and the proposed model highlight that intimate contact phenomenon at T_g can only happen if the material is amorphous enough. At this temperature the intimate contact phenomenon is a consequence of the deformation or flattening of the surface roughness between adjacent layers owing to the matrix change from its glassy state to rubbery state. Nevertheless, the final interlaminar consolidation quality which was evaluated by ILSS tests was similar for all the different crystallinity degrees.

Owing to this analysis of the consolidation phenomenon, optimal prepreg materials can be designed for OoA process, in terms of the initial crystallinity degree of matrix. Indeed, this parameter can be designed for triggering the intimate contact

creation sooner or later. In this way, for high-crystalline prepreg the intimate contact is delayed which allows to keep open interlaminar channels where internal voids can be evacuated.

Many work perspectives can be considered. An improvement of the intimate contact simulation can be done by coupling a heat transfer simulation with the mechanical deformation simulation which was presented in this article. Moreover, a study of surface roughness deformation linked to the crystallisation modelling would improve the model predictions. The viscoelastic behaviour of the matrix above T_g could be also considered whereas the elastic model was adopted for the matrix property. Finally, a study of internal porosity evacuation in a function of the crystallinity degree and of the prepreg microstructure could be helpful to select the optimal prepreg for vacuum-bag-only applications.

Data availability statement

The raw data supporting the conclusions of this article will be made available by the authors, without undue reservation.

Author contributions

FS, CS, and PB contributed to the design of experimental works and realized them. CHP supervised the research work. All the authors contributed to the development of the model, the interpretation of the results, the statistical analysis, and contributed to conception of the study.

Conflict of interest

The authors declare that the research was conducted in the absence of any commercial or financial relationships that could be construed as a potential conflict of interest.

Publisher's note

All claims expressed in this article are solely those of the authors and do not necessarily represent those of their affiliated organizations, or those of the publisher, the editors and the reviewers. Any product that may be evaluated in this article, or claim that may be made by its manufacturer, is not guaranteed or endorsed by the publisher.

References

- Akkerman, R., Bouwman, M., and Wijskamp, S. (2020). Analysis of the thermoplastic composite overmolding process: Interface strength. *Front. Mat.* 7, 2020. doi:10.3389/fmats.2020.00027
- Akkerman, R., and Haanappel, S. P. (2015). "6 - Thermoplastic composites manufacturing by thermoforming", in *Advances in composites manufacturing and process design*, Boisse, P., Ed. Woodhead Publishing, p.p 111–129. doi:10.1016/B978-1-78242-307-2.00006-3
- Armagan, A. (2020). "Effects of crystallization on mechanical properties of carbon fibre reinforced poly(ether ether ketone) composites," presented at the ICCM12. Paris, France, July, 1999.
- Bandaru, A. K., Clancy, G., Peeters, D., O'Higgins, R. M., and Weaver, P. M. (2019). Properties of a thermoplastic composite skin-stiffener interface in a stiffened structure manufactured by laser-assisted tape placement with *in situ* consolidation. *Compos. Struct.* 214, 123–131. avr. doi:10.1016/j.compstruct.2019.02.011
- Barnes, J. A., and Cogswell, F. N. (1989). Transverse flow processes in continuous fibre-reinforced thermoplastic composites. *Composites* 20 (1), 38–42. doi:10.1016/0010-4361(89)90680-0
- Batista, N. L., Olivier, P., Bernhart, G., Rezende, M. C., and Botelho, E. C. (2016). Correlation between degree of crystallinity, morphology and mechanical properties of PPS/carbon fiber laminates. *Mat. Res.* 19 (1), 195–201. févr. doi:10.1590/1980-5373-MR-2015-0453
- Blond, D., Vieille, B., Gomina, M., and Taleb, L. (2014). Correlation between physical properties, microstructure and thermo-mechanical behavior of PPS-based composites processed by stamping. *J. Reinf. Plast. Compos.* 33 (17), 1656–1668. doi:10.1177/0731684414541846
- Butler, C. A., McCullough, R. L., Pitchumani, R., and Gillespie, J. W. (1998). An analysis of mechanisms governing fusion bonding of thermoplastic composites. *J. Thermoplast. Compos. Mat.* 11 (4), 338–363. doi:10.1177/089270579801100404
- Cassidy, S. F., and Monaghan, P. F. (1994). Effect of contact resistances on the thermal conductivity of an unconsolidated fibre-reinforced thermoplastic prepreg stack. *Compos. Manuf.* 5 (4), 225–230. déc. doi:10.1016/0956-7143(94)90137-6
- Çelik, O., Peeters, D., Dransfeld, C., and Teuwen, J. (2020). Intimate contact development during laser assisted fiber placement: Microstructure and effect of process parameters. *Compos. Part A Appl. Sci. Manuf.* 134, 105888. juill. doi:10.1016/j.compositesa.2020.105888
- Chen, Q., Boisse, P., Park, C. H., Saouab, A., and Bréard, J. (2011). Intra/inter-ply shear behaviors of continuous fiber reinforced thermoplastic composites in thermoforming processes. *Compos. Struct.* 93 (7), 1692–1703. doi:10.1016/j.compstruct.2011.01.002
- Choupin, T., Fayolle, B., Régnier, G., Paris, C., Cinquin, J., and Brulé, B. (2018). A more reliable DSC-based methodology to study crystallization kinetics: Application to poly(ether ether ketone) (PEKK) copolymers. *Polymer* 155, 109–115. doi:10.1016/j.polymer.2018.08.060
- Choupin, T. (2017). "Mechanical performances of PEKK thermoplastic composites linked to their processing parameters," These de doctorat, Paris, ENSAM. Available at: <https://www.theses.fr/2017ENAM0043> (Accessed November 03, 2022).
- Costa, A., Botelho, E., Costa, M., Narita, N., and Tarpani, J. (2012). A review of welding technologies for thermoplastic composites in aerospace applications. *J. Aerosp. Technol. Manag.* 4, 255–266. doi:10.5028/jatm.2012.040303912
- De Gennes, P. G., « The formation of polymer/polymer junctions », in *Tribol. Ser.*, vol. 7, Georges, J. M., Éd. Elsevier, 1981, p. 355–367.
- Dörr, D., Joppich, T., Kugele, D., Henning, F., and Kärger, L. (2019). A coupled thermomechanical approach for finite element forming simulation of continuously fiber-reinforced semi-crystalline thermoplastics. *Compos. Part A Appl. Sci. Manuf.* 125, 105508. doi:10.1016/j.compositesa.2019.105508
- Dubary, N., Taconet, G., Bouvet, C., and Vieille, B. (2017). Influence of temperature on the impact behavior and damage tolerance of hybrid woven-ply thermoplastic laminates for aeronautical applications. *Compos. Struct.* 168, 663–674. doi:10.1016/j.compstruct.2017.02.040
- Engelhardt, R., Ehard, S., Wolf, T., Oelhafen, J., Kollmannsberger, A., and Drechsler, K. (2019). *In situ* joining of unidirectional Tapes on long fiber reinforced thermoplastic structures by thermoplastic automated fiber placement for scientific sounding rocket applications. *Procedia CIRP* 85, 189–194. janv. doi:10.1016/j.procir.2019.09.015
- Gardner, K. H., Hsiao, B. S., Matheson, R. R., and Wood, B. A. (1992). Structure, crystallization and morphology of poly (aryl ether ketone ketone). *Polymer* 33 (12), 2483–2495. doi:10.1016/0032-3861(92)91128-O
- Groves, D. J., and Stocks, D. M. (1991). Rheology of thermoplastic-carbon fibre composite in the elastic and viscoelastic states. *Compos. Manuf.* 2 (3), 179–184. janv. 1991. doi:10.1016/0956-7143(91)90137-6
- Grunenfelder, L. K., Dills, A., Centea, T., and Nutt, S. (2017). Effect of prepreg format on defect control in out-of-autoclave processing. *Compos. Part A Appl. Sci. Manuf.* 93, 88–99. févr. doi:10.1016/j.compositesa.2016.10.027
- Guan, X., and Pitchumani, R. (2004). Modeling of spherulitic crystallization in thermoplastic tow-placement process: Heat transfer analysis. *Compos. Sci. Technol.* 64 (9), 1123–1134. juill. doi:10.1016/j.compscitech.2003.08.011
- Guan, X., and Pitchumani, R. (2004). Modeling of spherulitic crystallization in thermoplastic tow-placement process: Spherulitic microstructure evolution. *Compos. Sci. Technol.* 64 (9), 1363–1374. juill. doi:10.1016/j.compscitech.2003.10.023
- Guzman-Maldonado, E., Hamila, N., Naouar, N., Moulin, G., and Boisse, P. (2016). Simulation of thermoplastic prepreg thermoforming based on a visco-hyperelastic model and a thermal homogenization. *Mat. Des.* 93, 431–442. doi:10.1016/j.matdes.2015.12.166
- Hsiao, B. S., Chang, I. Y., and Sauer, B. B. (1991). Isothermal crystallization kinetics of poly(ether ketone ketone) and its carbon-fibre-reinforced composites. *Polymer* 32 (15), 2799–2805. janv. doi:10.1016/0032-3861(91)90111-U
- Ijaz, M., Robinson, M., and Gibson, A. G. (2007). Cooling and crystallisation behaviour during vacuum-consolidation of commingled thermoplastic composites. *Compos. Part A Appl. Sci. Manuf.* 38 (3), 828–842. mars. doi:10.1016/j.compositesa.2006.08.007
- Judovits, L. (2020). "Thermal analysis of poly(aryl ether ketone) fibers," in *Thermal analysis of textiles and fibers*, pp. 247–258. doi:10.1016/B978-0-08-100572-9.00014-8
- Khan, M. A., Mitschang, P., and Schledjewski, R. (2010). Identification of some optimal parameters to achieve higher laminate quality through tape placement process. *Adv. Polym. Technol.* 29 (2), 98–111. doi:10.1002/adv.20177
- Kim, D., Centea, T., and Nutt, S. R. (2014). *In-situ* cure monitoring of an out-of-autoclave prepreg: Effects of out-time on viscosity, gelation and vitrification. *Compos. Sci. Technol.* 102, 132–138. doi:10.1016/j.compscitech.2014.07.027
- Kourkoutsaki, T., Comas-Cardona, S., Binetruy, C., Upadhyay, R. K., and Hinterhoelzl, R. (2015). The impact of air evacuation on the impregnation time of Out-of-Autoclave prepreps. *Compos. Part A Appl. Sci. Manuf.* 79, 30–42. déc. doi:10.1016/j.compositesa.2015.08.034
- Kratz, J., and Hubert, P. (2013). Anisotropic air permeability in out-of-autoclave prepreps: Effect on honeycomb panel evacuation prior to cure. *Compos. Part A Appl. Sci. Manuf.* 49, 179–191. doi:10.1016/j.compositesa.2013.02.013
- Krishnaswamy, R. K., and Kalika, D. S. (1996). Glass transition characteristics of poly(aryl ether ketone ketone) and its copolymers. *Polymer* 37 (10), 1915–1923. doi:10.1016/0032-3861(96)87309-5
- Laméthe, J.-F., Beauchêne, P., and Léger, L. (2005). Polymer dynamics applied to PEEK matrix composite welding. *Aerosp. Sci. Technol.* 9 (3), 233–240. avr. doi:10.1016/j.ast.2005.01.008
- Levy, A., Heider, D., Tierney, J., and Gillespie, J. W. (2013). Inter-layer thermal contact resistance evolution with the degree of intimate contact in the processing of thermoplastic composite laminates. *J. Compos. Mat.* 48, 491–503. doi:10.1177/0021998313476318
- Levy, A., Kratz, J., and Hubert, P. (2015). Air evacuation during Vacuum-Bag-Only prepreg processing of honeycomb sandwich structures: In-plane air extraction prior to cure. *Compos. Part A Appl. Sci. Manuf.* 68, 365–376. janv. doi:10.1016/j.compositesa.2014.10.013
- Li, C., and Strachan, A. (2019). Prediction of PEKK properties related to crystallization by molecular dynamics simulations with a united-atom model. *Polymer* 174, 25–32. doi:10.1016/j.polymer.2019.04.053
- Liebsch, A., Koshukow, W., Gebauer, J., Kupfer, R., and Gude, M. (2019). Overmoulding of consolidated fibre-reinforced thermoplastics - increasing the bonding strength by physical surface pre-treatments. *Procedia CIRP* 85, 212–217. déc. doi:10.1016/j.procir.2019.09.047
- Liu, L., Zhang, B.-M., Wang, D.-F., and Wu, Z.-J. (2006). Effects of cure cycles on void content and mechanical properties of composite laminates. *Compos. Struct.* 73 (3), 303–309. doi:10.1016/j.compstruct.2005.02.001
- Liu, X., and Chen, F. (2016). A review of void formation and its effects on the mechanical performance of carbon fiber reinforced plastic. *Eng. Trans.* 64 (1), 33–51.

- Loos, A. C., and Dara, P. H. (1987). "Processing of thermoplastic matrix composites," in *Review of progress in quantitative nondestructive evaluation* (Boston, MA, 1257–1265. doi:10.1007/978-1-4613-1893-4_143
- Lystrup, A., and Andersen, T. L. (1998). Autoclave consolidation of fibre composites with a high temperature thermoplastic matrix. *J. Mat. Process. Technol.* 77 (1), 80–85. doi:10.1016/S0924-0136(97)00398-1
- Mantell, S. C., and Springer, G. S. (1992). Manufacturing process models for thermoplastic composites. *J. Compos. Mat.* 26 (16), 2348–2377. janv. doi:10.1177/002199839202601602
- Margossian, A., Bel, S., and Hinterhoelzl, R. (2016). On the characterisation of transverse tensile properties of molten unidirectional thermoplastic composite tapes for thermoforming simulations. *Compos. Part A Appl. Sci. Manuf.* 88, 48–58. doi:10.1016/j.compositesa.2016.05.019
- Marsh, G. (2014). Reinforced thermoplastics, the next wave? *Reinf. Plast.* 58 (4), 24–28. doi:10.1016/S0034-3617(14)70177-8
- Martineau, L., Chabert, F., Boniface, B., and Bernhart, G. (2019). Effect of interfacial crystalline growth on autohesion of PEEK. *Int. J. Adhes. Adhes.* 89, 82–87. doi:10.1016/j.ijadhadh.2018.11.013
- McIlhagger, A., Archer, E., and McIlhagger, R. (2015). "3 - Manufacturing processes for composite materials and components for aerospace applications," in *Polymer composites in the aerospace industry*. Editors P. E. Irving and C. Soutis (Woodhead Publishing), pp. 53–75. doi:10.1016/B978-0-85709-523-7.00003-7
- Mulye, P. D., Hemmer, J., Morancay, L., Binetruy, C., Leygue, A., Comas-Cardona, S., et al. (2020). Numerical modeling of interply adhesion in composite forming of viscous discontinuous thermoplastic prepregs. *Compos. Part B Eng.* 191, 107953. juin 2020. doi:10.1016/j.compositesb.2020.107953
- Olivier, P., Cottu, J. P., and Ferret, B. (1995). Effects of cure cycle pressure and voids on some mechanical properties of carbon/epoxy laminates. *Composites* 26 (7), 509–515. doi:10.1016/0010-4361(95)96808-J
- Patou, J., Bonnaire, R., De Luycker, E., and Bernhart, G. (2019). Influence of consolidation process on voids and mechanical properties of powdered and commingled carbon/PPS laminates. *Compos. Part A Appl. Sci. Manuf.* 117, 260–275. doi:10.1016/j.compositesa.2018.11.012
- Picher-Martel, G.-P., Levy, A., and Hubert, P. (2017). Compression molding of Carbon/Polyether ether ketone composites: Squeeze flow behavior of unidirectional and randomly oriented strands. *Polym. Compos.* 38 (9), 1828–1837. doi:10.1002/pc.23753
- Qureshi, Z., Swait, T., Scaife, R., and El-Dessouky, H. M. (2014). *In situ* consolidation of thermoplastic prepreg tape using automated tape placement technology: Potential and possibilities. *Compos. Part B Eng.* 66, 255–267. doi:10.1016/j.compositesb.2014.05.025
- Régnier, G., Nicodeau, C., Verdu, J., Chinesta, F., Triquenaux, V., and Cinquin, J. (2005). "Welding of thermoplastic matrix composites: Prediction of macromolecules diffusion at the interface," in *8th ESAFORM conference on material forming*.
- Sadighi, M., Rabizadeh, E., and Kermansaravi, F. (2008). Effects of laminate sequencing on thermoforming of thermoplastic matrix composites. *J. Mat. Process. Technol.* 201 (1), 725–730. doi:10.1016/j.jmatprotec.2007.11.239
- Saffar, F., Sonnenfeld, C., Beauchêne, P., and Park, C. H. (2020). *In-situ* monitoring of the out-of-autoclave consolidation of carbon/Poly-Ether-Ketone-Ketone prepreg laminate. *Front. Mat.* 7, 195. doi:10.3389/fmats.2020.00195
- Schaefer, P., Guglhoer, T., Sause, M., and Drechsler, K. (2017). Development of intimate contact during processing of carbon fiber reinforced Polyamide-6 tapes. *J. Reinf. Plast. Compos.* 36 (8), 593–607. avr. doi:10.1177/0731684416687041
- Schechter, S. G. K., Centea, T., and Nutt, S. (2020). Effects of resin distribution patterns on through-thickness air removal in vacuum-bag-only prepregs. *Compos. Part A Appl. Sci. Manuf.* 130, 105723. doi:10.1016/j.compositesa.2019.105723
- Schechter, S. G. K., Centea, T., and Nutt, S. R. (2018). Polymer film dewetting for fabrication of out-of-autoclave prepreg with high through-thickness permeability. *Compos. Part A Appl. Sci. Manuf.* 114, 86–96. doi:10.1016/j.compositesa.2018.08.002
- Schuhler, E., Coppalle, A., Vieille, B., Yon, J., and Carpier, Y. (2018). Behaviour of aeronautical polymer composite to flame: A comparative study of thermoset- and thermoplastic-based laminate. *Polym. Degrad. Stab.* 152, 105–115. doi:10.1016/j.polymdegradstab.2018.04.004
- Shin, J. H., Kim, D., Centea, T., and Nutt, S. R. (2019). Thermoplastic prepreg with partially polymerized matrix: Material and process development for efficient part manufacturing. *Compos. Part A Appl. Sci. Manuf.* 119, 154–164. avr. doi:10.1016/j.compositesa.2019.01.009
- Soutis, C. (2020). "Aerospace engineering requirements in building with composites," in *Polymer composites in the aerospace industry*, pp. 3–22. doi:10.1016/B978-0-08-102679-3.00001-0
- Stanley, W., and Mallon, P. (2006). Intraply shear characterisation of a fibre reinforced thermoplastic composite. *Compos. Part A Appl. Sci. Manuf.* 37, 939–948. doi:10.1016/j.compositesa.2005.03.017
- Stewart, R. (2011). Thermoplastic composites — Recyclable and fast to process. *Reinf. Plast.* 55 (3), 22–28. doi:10.1016/S0034-3617(11)70073-X
- Stokes-Griffin, C. M., and Compston, P. (2015). A combined optical-thermal model for near-infrared laser heating of thermoplastic composites in an automated tape placement process. *Compos. Part A Appl. Sci. Manuf.* 75, 104–115. août 2015. doi:10.1016/j.compositesa.2014.08.006
- Tadini, P., Grange, N., Chetehouna, K., Gascoin, N., Senave, S., and Reynaud, I. (2017). Thermal degradation analysis of innovative PEKK-based carbon composites for high-temperature aeronautical components. *Aerosp. Sci. Technol.* 65, 106–116. doi:10.1016/j.ast.2017.02.011
- Talbot, M. F., Springer, G. S., and Berglund, L. A. (2016). The effects of crystallinity on the mechanical properties of PEEK polymer and graphite fiber reinforced PEEK. *J. Compos. Mat.* 21, 1056–1081. doi:10.1177/002199838702101104
- Tannous, M., Barasinski, A., Binetruy, C., and Courtemanche, B. (2016). Contribution of thermo-mechanical parameters and friction to the bonding of thermoplastic tapes in the tape winding process. *J. Mat. Process. Technol.* 229, 587–595. doi:10.1016/j.jmatprotec.2015.10.013
- Tierney, J. J., and Gillespie, J. W., Jr. (2004). Crystallization kinetics behavior of PEEK based composites exposed to high heating and cooling rates. *Compos. Part A Appl. Sci. Manuf.* 35 (5), 547–558. doi:10.1016/j.compositesa.2003.12.004
- Wang, P., Hamila, N., and Boisse, P. (2013). Thermoforming simulation of multilayer composites with continuous fibres and thermoplastic matrix. *Compos. Part B Eng.* 52, 127–136. doi:10.1016/j.compositesb.2013.03.045
- Wisnom, M. R., Reynolds, T., and Gwilliam, N. (1996). Reduction in interlaminar shear strength by discrete and distributed voids. *Compos. Sci. Technol.* 56 (1), 93–101. janv. doi:10.1016/0266-3538(95)00128-X
- WooLee, Il, and Springer, G. S. (1987). A model of the manufacturing process of thermoplastic matrix composites. *J. Compos. Mat.* 21 (11), 1017–1055. doi:10.1177/002199838702101103
- Wypych, G. (2012). "PEKK polyetherketoneketone," in *Handbook of polymers*. Editor G. Wypych, pp. 367–369. doi:10.1016/B978-1-895198-47-8.50111-9
- Xu, T., Yu, J., and Jin, Z. (2001). Effects of crystalline morphology on the impact behavior of polypropylene. *Mat. Des.* 22 (1), 27–31. févr. doi:10.1016/S0261-3069(00)00033-9
- Yang, F., and Pitchumani, R. (2001). A fractal Cantor set based description of interlaminar contact evolution during thermoplastic composites processing. *J. Mat. Sci.* 36 (19), 4661–4671. doi:10.1023/A:1017950215945